SU(12) Kondo effect in a carbon nanotube quantum dot

Igor Kuzmenko and Yshai Avishai
Department of Physics, Ben-Gurion University of the Negev, Beer-Sheva, Israel
(Received 26 November 2013; revised manuscript received 9 March 2014; published 8 May 2014)

We study the Kondo effect in a CNT(left lead)-CNT(QD)-CNT(right lead) structure. Here CNT is a single-wall metallic carbon nanotube, for which (1) the valence and conduction bands of electrons with zero orbital angular momentum ($m = 0$) coalesce at the two valley points **K** and **K**′ of the first Brillouin zone and (2) the energy spectrum of electrons with $m \neq 0$ has a gap whose size is proportional to $|m|$. Following adsorption of hydrogen atoms and application of an appropriately designed gate potential, electron energy levels in the CNT(QD) are tunable to have (1) twofold spin degeneracy; (2) twofold isospin (valley) degeneracy; and (3) threefold orbital degeneracy $m = 0, \pm 1$. As a result, an SU(12) Kondo effect is realized with remarkably high Kondo temperature. Unlike the SU(2) case, the low temperature conductance and magnetic susceptibility have a peak at finite temperature. Moreover, the magnetic susceptibilities for parallel and perpendicular magnetic fields (with respect to the tube axis) display anisotropy with a universal ratio $\chi^{\parallel}_{\rm imp}/\chi^{\perp}_{\rm imp} = \eta$ that depends only on the electron's orbital and spin g factors.

DOI: 10.1103/PhysRevB.89.195110 PACS number(s): 73.21.Hb, 73.21.La, 73.22.Dj, 73.23.Hk

I. INTRODUCTION

Background: Kondo tunneling through carbon nanotube quantum dots [CNT(QD)] has recently become a subject of intense theoretical [1–6] and experimental [7–12] studies. One of the motivations for pursuing this research direction is the quest for achieving an exotic Kondo effect with SU(N) dynamical symmetry [13–17], based on the peculiar properties of electron spectrum in CNT [18,19]. Achieving SU(4) symmetry is natural because the energy spectrum of metallic CNT consists of two independent valleys that touch at the **K** and **K**′ points of the Brillouin zone. The energy levels possess degeneracy in both spin ($\uparrow,\downarrow$) and isospin (or valley **K**,**K**′) quantum numbers. Thus, due to both spin and isospin degeneracy, an SU(4) Kondo effect takes place [1–3,10–12].

Motivation: Achieving even higher degeneracy SU($N > 4$) of the QD is highly desirable. First, the Kondo temperature dramatically increases with N. Second, there is a hope to expose novel physical observables that are peculiar to these higher symmetries. In the present device, higher degeneracy may be obtained by employing the orbital (cylindrical) symmetry of electron states in CNT, an option which so far has not been effectively employed in this quest. In order to manipulate these orbital features, we use the fact that adsorption of oxygen, hydrogen, or fluorine atoms on the surface of the CNT gives rise to a gap opening in the spectrum of the metallic CNT [20,21]. Realization of SU($N > 4$) Kondo effect then becomes feasible, since there is now spin, isospin (valley), and orbital degeneracy.

The main objectives: The main goals of the present work are (1) to show that SU(12) Kondo effect in the CNT(left lead)-CNT(QD)-CNT(right lead) structure is indeed achievable and (2) to elucidate the physical content of this structure at the Kondo regime as encoded by tunneling conductance and the magnetic susceptibility. The first goal is obtained by designing the electron spectrum in the CNT(QD) to have a 12-fold degeneracy following adsorption of hydrogen atoms combined with an application of a nonuniform gate potential. Namely, the energy levels of the central element CNT(QD) are tunable into a threefold orbital degeneracy for $m = 0, \pm 1$ (where m is the component of the orbital angular momentum along the CNT axis). The second goal is achieved through quantitative analysis, based on perturbation theory at high temperatures and mean field slave boson formalism at low temperature.

The main results: The energy spectrum of the CNT(QD) gated by a spatially modulated potential is elucidated, and the possibility to get a CNT(QD) with 12-fold degenerate quantum states is substantiated. This CNT(QD) is then integrated into a tunneling junction CNT(left lead)-CNT(QD)-CNT(right lead) as shown in Fig. 1. When the ground state of the interacting CNT(QD) is occupied by a single electron, Kondo tunneling with SU(12) dynamical symmetry is realized. This exotic Kondo effect is quantitatively analyzed. First, the corresponding Kondo temperature is calculated and shown to be much higher than in the standard SU(2) Kondo effect. The tunneling conductance $G(T)$ and the magnetic susceptibilities $\chi^{\parallel}_{\rm imp}(T)$, $\chi^{\perp}_{\rm imp}(T)$ for respective magnetic fields parallel and perpendicular to the CNT axis are calculated in the weak ($T \gg T_K$) and strong ($T < T_K$) coupling regimes.

The low temperature dependencies of both $G(T)$ and $\chi(T)$ are entirely distinct from their analogs pertaining to the SU(2) Kondo effect in quantum dot [22]. More concretely, the temperature dependence of both quantities is shown to have a peak at *finite temperature*, unlike the familiar monotonic behavior encountered in the ordinary SU(2) Kondo effect in quantum dots. Moreover, inspection of the magnetic susceptibility exposes an observable peculiar to the SU(12) symmetry [or other SU(N) symmetry with $N > 2$]: It is shown that the magnetic response is anisotropic, that is, $\chi^{\parallel}_{\rm imp}(T) \neq \chi^{\perp}_{\rm imp}(T)$. Even more remarkable, the ratio $\eta \equiv \chi^{\parallel}_{\rm imp}(T)/\chi^{\perp}_{\rm imp}(T)$ is a "universal number" depending only on $g_{\rm orb}$ and $g_{\rm spin}$, that are the orbital and spin g factors of electrons in the CNT(QD) (and not on temperature).

These distinctions open the door for experimental manifestation of this peculiar junction. This is helped by the unusually high Kondo temperature that enables the measurement of the tunneling conductance in the Kondo regime at relatively high temperature.

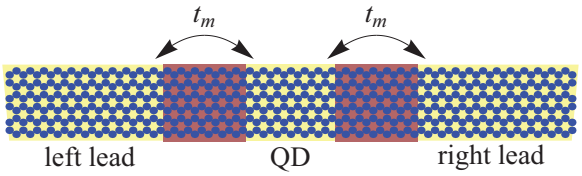

FIG. 1. (Color online) CNT(left lead)-CNT(QD)-CNT(right lead) junction.

Organization: This paper is structured as follows: In Sec. II we describe the basic structure of an infinitely long metallic CNT with adsorbed hydrogen atoms. The energy spectrum of the CNT(QD) is discussed in Sec. III. The Anderson model for the tunnel junction is introduced in Sec. IV, followed by Sec. V in which the Anderson Hamiltonian in the local moment regime is mapped on a spin Hamiltonian, poor-man scaling equations for the coupling constants are derived, and the Kondo temperature is evaluated. In Secs. VI and VII the results of our calculations of the tunneling conductance and the magnetic susceptibilities are, respectively, presented both in the weak and strong coupling regimes. The main achievements of the present work are summarized in Sec. VIII. Analysis of the electron wave functions in the CNT(QD) with adsorbed hydrogen atoms under the appropriate gate potential is relegated to Appendix A. Zeeman splitting for electrons in CNT subject to an external magnetic field is calculated in Appendix B. The ratio $\chi^{\parallel}_{\rm imp}(T)/\chi^{\perp}_{\rm imp}(T)$ is derived in Appendix C using the fluctuation-dissipation theorem.

II. MODEL

Characteristic energy dispersion relation for an electron in CNT is derivable from the special band structure of a graphene sheet [18,19,23,24]. Let $\mathbf{c}_{n_1 n_2}$ denote the chiral vector that represents a possible rolling of graphene into a CNT. When $n_1 - n_2$ is an integer multiple of 3, a CNT becomes a zero-gap semiconductor. Else, it becomes a semiconducting nanotube with a finite band gap [18,19]. The band structure of a metallic CNT exhibits two Dirac points with a right- and left-moving branch around each Dirac point. A peculiar consequence of the Dirac nature of charge carriers in CNT is that electrons can tunnel through a potential barrier without reflection [25]. This Klein paradox prevents a practical aspect of CNT: It is virtually impossible to trap an electron in between potential barriers, as it can escape out. It also hinders the formation of a gap in the band spectrum. Fortunately, this can be circumvented by chemical modification of the CNT. In Refs. [20,21] it is shown that when radicals such as atomic oxygen, hydrogen, or fluorine are adsorbed on the graphene surface they form covalent bonds with the carbon atoms. These covalent bonds are realized since the carbon atoms change their hybridization from sp^2 to sp^3, and that results in the opening of a band gap (similar to the situation in diamond crystals). Its size can reach $2\Delta_g \sim 1$ eV depending on the density of adsorbed atoms [20,26].

The energy spectrum of the metallic CNT with adsorbed atoms can adequately be approximated (at least at low energy) from that of a graphene sheet with adsorbed atoms using the formula

$$\varepsilon_{k_x k_y} = \sqrt{(\hbar v k_x)^2 + (\hbar v k_y)^2 + \Delta_g^2}. \tag{1}$$

In the above equation we keep k_x to be a continuous wave number for electron motion along the CNT axis and $k_y = m/r_0$ as a discrete wave number for the motion along the circumference direction. Here v is the Fermi velocity, r_0 is the CNT radius, and the integer m is an orbital quantum number. The energy spectrum of hydrogenated graphene measured in Ref. [27] is shown in Fig. 2. It is seen that Eq. (1) (dashed line) agrees well with experimental data.

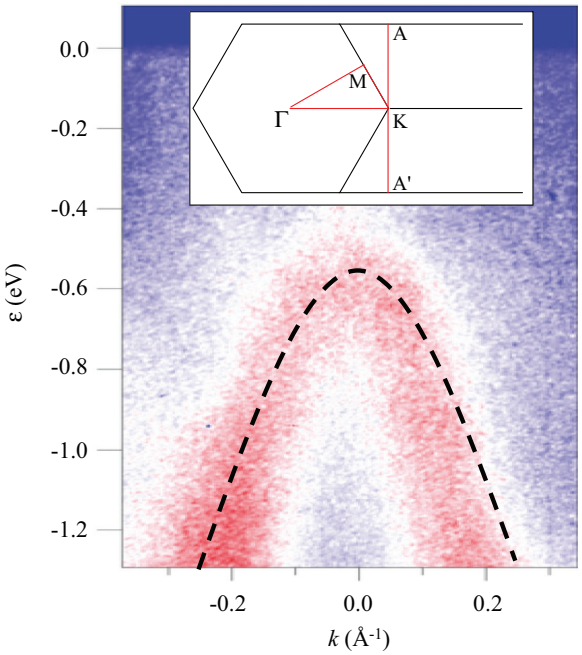

FIG. 2. (Color online) Observation of a gap opening in hydrogenated graphene. Density plot denotes photoemission intensity along the A-K-A' direction of the Brillouin zone (see inset) measured in Ref. [27], whereas the dashed line is the spectrum calculated according to Eq. (1). Inset: The Brillouin zone of graphene.

With the present experimental facilities, the density of adsorbed atoms can be manipulated to be dependent on x in such a way that the gap Δ_g is approximately given by the following function of x:

$$\Delta_g(x) = \begin{cases} M_0, & \text{if} \quad |x| < h \quad \text{or} \quad |x| > h + a, \\ N_0, & \text{if} \quad h < |x| < h + a, \end{cases} \tag{2}$$

where $N_0 > M_0$. The Fermi level ϵ_F is tuned to satisfy the inequality $N_0 > \epsilon_F > M_1$. Thereby, the CNT is divided into five intervals numbered 1–5, with the following respective electronic properties: Two intervals (1 and 5), with $|x| > h + a$, serve as left and right metallic leads. Two insulating intervals (2 and 4), with $h < |x| < h + a$, serve as left and right tunneling barriers. Finally, interval 3, with $|x| < h$, serves as quantum dot (see Fig. 3).

III. ENERGY LEVELS OF CNT(QD)

We describe the quantum states of electrons in the CNT in the long-wave $\mathbf{k} \cdot \mathbf{p}$ approximation. This approximation

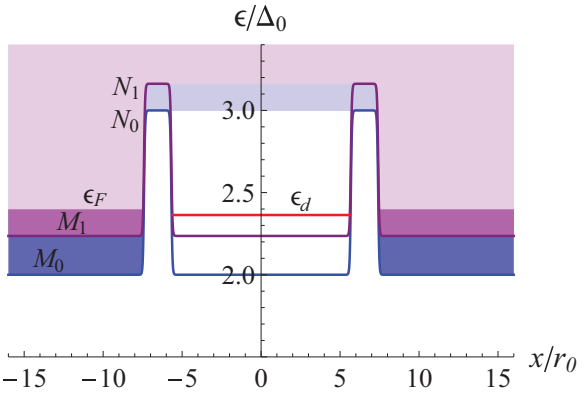

FIG. 3. (Color online) Left and right tunnel barriers separating left and right leads from the quantum dot. Here $M_0 = 2\Delta_0$, $M_1 = \sqrt{3}\Delta_0$, $N_0 = 3\Delta_0$, and $N_1 = \sqrt{10}\Delta_0$. The 12-fold degenerate level is $\varepsilon_d = 2.3635\Delta_0$ (red line) and the Fermi level is $\epsilon_F = 2.4013\Delta_0$. The QD half-length is $h = 5.6826r_0$ and the barrier width is $a = 1.73r_0$.

is good when the wave vector $\mathbf{k}$ of the electron is close to the $\mathbf{K}$ or $\mathbf{K}'$ point of the first Brillouin zone (BZ) of the hexagonal lattice of the CNT, i.e., when $|\mathbf{k} - \mathbf{K}| \ll K$ or $|\mathbf{k} - \mathbf{K}'| \ll K$ (see Fig. 4 for illustration). However, when an electron is rejected from the edges of the CNT QD, the possible transitions between the valleys $\mathbf{K}$ and $\mathbf{K}'$ cannot be described in the framework of long-wave approximation. Therefore, it will be useful to start our discussions from the microscopic tight-binding model [18,19].

A CNT is specified by a chiral vector

$$\mathbf{c}_{n_1n_2} = n_1\mathbf{a}_1 + n_2\mathbf{a}_2, \tag{3}$$

where $\mathbf{a}_1$ and $\mathbf{a}_2$ are the basis vectors ($|\mathbf{a}_1| = |\mathbf{a}_2| = a_0 = 2.46$ Å), and n_1 and n_2 are integers. A CNT is obtained by rolling a two-dimensional (2D) graphene sheet such that the atom at the origin coincides with the atom at $\mathbf{c}_{n_1n_2}$. Then $|\mathbf{c}_{n_1n_2}| = 2\pi r_0$ is the length of the CNT circumference and r_0 is the CNT radius. We specify the CNT by a chiral angle ϕ_0, the angle between $\mathbf{c}_{n_1n_2}$ and the basis vector $\mathbf{a}_1$, as shown in Fig. 4. The hexagonal symmetry of graphene gives us the condition $-\frac{\pi}{6} < \phi_0 \leqslant \frac{\pi}{6}$. Two special values of ϕ_0 are $\phi_0 = 0$ and $\phi_0 = \frac{\pi}{6}$. For $\phi_0 = 0$, a zigzag CNT is constructed, while for $\phi = \frac{\pi}{6}$, one has an armchair CNT [18,19].

When an electron is scattered off an effective potential given in Eq. (2), the component k_x of the 2D wave vector $\mathbf{k}$ is not a good quantum number, whereas k_y is still a good quantum number. As a result, for most types of nanotubes with $\phi_0 \neq \frac{\pi}{6}$ (that is, except armchair ones) the vectors $\mathbf{K}$ and $\mathbf{K}'$ are not collinear to the CNT axis [see Fig. 4(b)], and therefore the electron that is localized by the potential (2) can change its wave vector from $\mathbf{K} + \mathbf{q}$ to $\mathbf{K} - \mathbf{q}$ or from $\mathbf{K}' + \mathbf{q}$ to $\mathbf{K}' - \mathbf{q}$, and there is no quantum transitions between the valleys $\mathbf{K}$ and $\mathbf{K}'$. For an armchair CNT, the vectors $\mathbf{K}$ and $\mathbf{K}'$ are collinear with the axis of the CNT, and therefore there are quantum transitions from $\mathbf{K}$ to $\mathbf{K}'$ which lift the intervalley degeneracy. In what follows, we will consider the CNT QDs which possess the intervalley degeneracy (that is, $\phi_0 \neq \frac{\pi}{6}$).

When $|\mathbf{q}| \ll K$, the single electron wave functions and the corresponding energy spectrum of the CNT(QD) are deduced from the corresponding analog of the Dirac equation which in the present geometry takes the form

$$\tilde{H}_d\Phi_{mn}(x,\phi) = \epsilon\Phi_{mn}(x,\phi). \tag{4}$$

Here $\Phi_{mn}(x,\phi)$ is the wave function with principal quantum number n ($n = 1,2,3,\ldots$) and magnetic quantum number m ($m = 0,\pm1,\pm2,\ldots$). The Hamiltonian of the QD in the $\mathbf{k}\cdot\mathbf{p}$ approximation is $\tilde{H}_d = \mathbf{d}(x)\cdot\boldsymbol{\tau}$, where

$$\begin{aligned}\mathbf{d}(x) &= \mathbf{d}_{\rm in}\vartheta(h - |x|) + \mathbf{d}_{\rm out}\vartheta(|x| - h),\\ \mathbf{d}_{\rm in} &= \hbar v(\mathbf{e}_x k_x + \mathbf{e}_y k_y) + \mathbf{e}_z M_0,\\ \mathbf{d}_{\rm out} &= \hbar v(\mathbf{e}_x k_x + \mathbf{e}_y k_y) + \mathbf{e}_z N_0.\end{aligned}$$

Here $\boldsymbol{\tau} = (\tau_x,\tau_y,\tau_z)$ is the vector of Pauli matrices acting in the pseudospin space (corresponding to sublattices A and B),

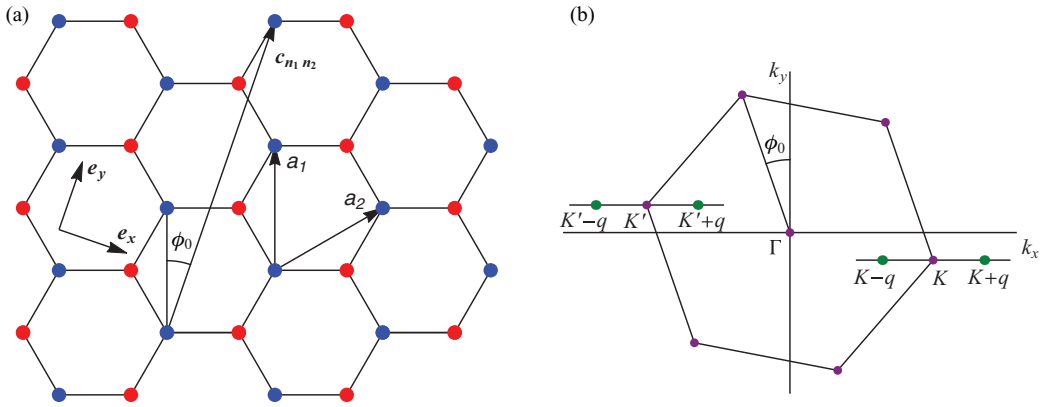

FIG. 4. (Color online) (a) A monoatomic layer of graphene. The red and blue dots denote carbon atoms of the sublattice A and B. The primitive vectors of graphene are $\mathbf{a}_1$ and $\mathbf{a}_2$. The nanotube is obtained by choosing the chiral vector $\mathbf{c}_{n_1n_2}$, Eq. (3). The unit vectors $\mathbf{e}_x$ and $\mathbf{e}_y$ are fixed in the CNT in such a way that $\mathbf{e}_x$ is along the CNT axis, and $\mathbf{e}_y$ is along the circumferential direction $\mathbf{c}_{n_1n_2}$. The chiral angle between $\mathbf{a}_1$ and $\mathbf{c}_{n_1n_2}$ is ϕ_0. (b) The first Brillouin zone of graphene. k_x is the component of the 2D wave vector $\mathbf{k}$ along the CNT axis and k_y is the component of $\mathbf{k}$ in the circumferential direction. The angle between $\mathbf{K}$ and the axis k_x is $\phi_0 - \frac{\pi}{6}$. $\mathbf{K} \pm \mathbf{q}$ and $\mathbf{K}' \pm \mathbf{q}$ (green dots) are degenerate quantum states in the valleys $\mathbf{K}$ and $\mathbf{K}'$.

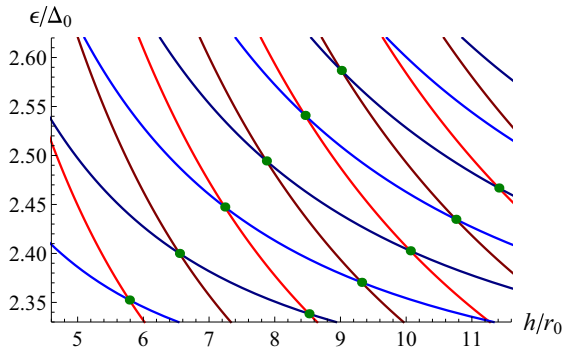

FIG. 5. (Color online) Parametric diagram ϵ-h describing energies ϵ of the discrete levels of the quantum dot for $m = 0$ (light red and dark red curves) and $m = \pm 1$ (light blue and dark blue curves) and different values of the CNT(QD) half-length h. The crossing points (green dots) denote energies with threefold orbital degeneracy for which SU(12) symmetry is expected. Here we use $M_0 = 2\Delta_0$ and $N_0 = 3\Delta_0$. The light red and light blue curves correspond to even principal quantum number n and dark red and dark blue curves correspond to odd n.

$\vartheta(x)$ is the step function, and

$$k_x = -i\partial_x, \quad k_y = -\frac{i}{r_0}\partial_\phi. \tag{5}$$

The function $\Phi_{mn}(x)$ is calculated in Appendix A. The energy levels of the QD are obtained by solving the equation

$$\mathcal{F}_\downarrow(\epsilon)\sqrt{\epsilon + M_m}\cos\left(k_x h + \frac{n\pi}{2}\right) = \mathcal{F}_\uparrow(\epsilon)\sqrt{\epsilon - M_m}\sin\left(k_x h + \frac{n\pi}{2}\right), \tag{6}$$

where

$$\mathcal{F}_\sigma(\epsilon) = \sum_{\sigma'} \frac{\sqrt{\epsilon(N_m + \sigma'\epsilon)}}{\sqrt{2N_m}}\left(\chi_\sigma^{(1)} \cdot \chi_{\sigma'}^{(2)}\right). \tag{7}$$

$\chi_\sigma^{(\nu)}$ ($\nu = 1,2$) are eigenspinors of the operators

$$\hat{M}_m^\nu = m\Delta_0\tau_y + M_0^\nu\tau_z,$$

$M_m^1 = M_m$, $M_m^2 = N_m$. Explicitly,

$$\chi_\uparrow^{(\nu)} = \frac{1}{\sqrt{2M_m^\nu\left(M_m^\nu + M_0^\nu\right)}}\begin{pmatrix} M_m^\nu + M_0^\nu \\ im\Delta_0 \end{pmatrix}, \tag{8}$$

$\chi_\downarrow^{(\nu)} = i\tau^x\chi_\uparrow^{(\nu)}$.

The energy spectrum of the QD for different values of the dot length $2h$ is shown in Fig. 5. The red or blue curves denote energy levels for $m = 0$ or $m = \pm 1$ and different spatial parities. The light red and light blue curves describe quantum states with even principal quantum number n (the wave functions of such states are symmetric with respect to the inversion $x \to -x$), whereas the dark red and dark blue curves correspond to odd n. The level crossing points (green dots) are threefold (orbital) degenerate. At these points, SU(12) symmetry is expected.

IV. ANDERSON MODEL

We now consider the tunnel junction consisting of left and right CNT metallic leads (CNT), and a CNT quantum dot (QD), as shown in Fig. 1. The Anderson Hamiltonian of the CNT-CNT (QD)-CNT junction has the form

$$H = H_0 + H_t, \quad H_0 = H_l + H_r + H_d, \tag{9}$$

$$H_\alpha = \sum_{k\lambda}\epsilon_{km}c_{\alpha k\lambda}^\dagger c_{\alpha k\lambda}, \quad \alpha = l,r, \tag{10}$$

$$H_d = \epsilon_d\sum_\lambda d_\lambda^\dagger d_\lambda + U_d\hat{N}_d(\hat{N}_d - 1), \tag{11}$$

$$H_t = \sum_{\alpha\lambda} t_m\{\psi_{\alpha\lambda}^\dagger d_\lambda + \text{H.c.}\}, \tag{12}$$

where

$$\hat{N}_d = \sum_\lambda d_\lambda^\dagger d_\lambda.$$

Here $\lambda = \{\xi, m, \sigma\}$, where $\xi = \mathbf{K}, \mathbf{K}'$ (the isospin) corresponds to electrons with wave vectors near the $\mathbf{K}$ and $\mathbf{K}'$ corner points in the 2D Brillouin zone, m is the magnetic quantum number, and σ is the spin. Finally, $\psi_{\alpha\lambda} \equiv \psi_{\alpha\lambda}(x = 0)$ is a field operator at $x = 0$,

$$\psi_{\alpha\lambda}(x) = \frac{1}{\sqrt{L_{\text{cnt}}}}\sum_k c_{\alpha k\lambda}e^{ikx},$$

L_{cnt} is the length of the CNT lead. The tunneling rates t_m are estimated as

$$t_m \cong \frac{\hbar v}{\sqrt{h}}\frac{M_m}{\epsilon_F}\exp\left\{-\frac{a}{\hbar v}\sqrt{N_m^2 - \epsilon_F^2}\right\}.$$

We choose the parameters N_0, ϵ_F, and a such that the resonance width

$$\Gamma = 4\pi t_m^2\rho_m(\epsilon_F) \tag{13}$$

does not depend on m. Here $\rho_m(\epsilon)$ is the density of states of electrons with magnetic quantum number m,

$$\rho_m(\epsilon) = \frac{|\epsilon|\vartheta(|\epsilon| - M_m)}{2\pi\hbar v\sqrt{\epsilon^2 - M_m^2}}. \tag{14}$$

V. SPIN HAMILTONIAN, SCALING EQUATIONS, AND KONDO TEMPERATURE

The properly tuned CNT(QD) in its ground state has one electron whose energy ε_d is 12-fold degenerate ($m = 0, \pm 1$, $\xi = \mathbf{K}, \mathbf{K}'$, and $\sigma = \uparrow, \downarrow$). Tunneling of electrons between the CNT(QD) and the CNT leads, encoded by H_t [Eq. (12)], changes the number of electrons in the dot. In the local moment regime, the Schrieffer-Wolff transformation is then used [28,29] to project out zero and two electron states ($|0\rangle$ and $|\lambda\lambda'\rangle$). It maps the Hamiltonian H [Eq. (9)] onto an effective Hamiltonian $\tilde{H} = H_l + H_r + H_K$. Here H_K, the Coqblin-Shrieffer spin Hamiltonian with the dot states $|0\rangle$ and

$|\lambda\lambda'\rangle$ frozen out, has the following form [29,30]:

$$H_K = \frac{1}{24}\sum_{\alpha\alpha'}\sum_{\lambda} K_{mm}\psi^\dagger_{\alpha'\lambda}\psi_{\alpha\lambda} + \frac{1}{2}\sum_{\alpha\alpha'}\sum_{\lambda} J_{mm}Z^{\lambda\lambda}\psi^\dagger_{\alpha'\lambda}\psi_{\alpha\lambda} + \frac{1}{2}\sum_{\alpha\alpha'}\sum_{\lambda\neq\lambda'} J_{mm'}X^{\lambda\lambda'}\psi^\dagger_{\alpha'\lambda'}\psi_{\alpha\lambda}, \quad (15)$$

where $X^{\lambda\lambda'} = |\lambda\rangle\langle\lambda'|$ are Hubbard operators coupling different degenerate dot states, and

$$Z^{\lambda\lambda} = X^{\lambda\lambda} - \frac{1}{N}\sum_{\lambda'} X^{\lambda'\lambda'}, \quad N = 12.$$

The couplings K_{mm} and $J_{mm'}$ are

$$\begin{aligned} J_{mm'} &= J^{(1)}_{mm'} + J^{(2)}_{mm'}, \\ K_{mm} &= J^{(1)}_{mm'} - (N-1)J^{(2)}_{mm'}, \\ J^{(1)}_{mm'} &= \frac{2t_m t_{m'}}{\epsilon_F - \epsilon_d}, \\ J^{(2)}_{mm'} &= \frac{2t_m t_{m'}}{U_d - \epsilon_F + \epsilon_d}. \end{aligned}$$

Employing the simplifying assumption (13) we introduce the dimensionless coupling constant

$$\begin{aligned} j &= J_{mm'}\sqrt{\rho_m(\epsilon_F)\rho_{m'}(\epsilon_F)} \\ &= \frac{U_d\Gamma}{2\pi(\epsilon_F - \epsilon_d)(U_d - \epsilon_F + \epsilon_d)} > 0. \end{aligned} \quad (16)$$

By Eq. (13) j does not depend on the orbital quantum number m while $J_{mm'}$ and ρ_m do. Within the standard poor man's scaling technique, the coupling $j(D)$ is renormalized as the original bandwidth $\bar{D}$ is reduced to $D < \bar{D}$ by integrating out high energy excitations. Within the same assumption on Γ, the constants K_{mm} are not renormalized and therefore the interaction terms proportional to K_{mm} can be considered as part of potential scattering.

The scaling equation for $j(D)$ supported by the initial condition at $\bar{D}$ reads

$$\begin{aligned} \frac{\partial j}{\partial \ln D} &= -\frac{Nj^2}{2}, \\ j(\bar{D}) &= \frac{U_d\Gamma}{2\pi(\epsilon_F - \epsilon_d)(U_d - \epsilon_F + \epsilon_d)}. \end{aligned} \quad (17)$$

Equation (17) has the solution

$$j(T) = \frac{2}{N\ln(T/T_K)}, \quad (18)$$

where the Kondo temperature (the scaling invariant of the RG equation) is given by

$$T_K = \bar{D}\exp\left[-\frac{4\pi(\epsilon_F - \epsilon_d)(U_d - \epsilon_F + \epsilon_d)}{NU_d\Gamma}\right]. \quad (19)$$

The argument of the exponent is six times smaller than the one obtained for SU(2) Kondo effect, implying the $T_K[\mathrm{SU}(12)] \gg T_K[\mathrm{SU}(2)]$.

VI. CONDUCTANCE

In this section we will calculate the tunneling conductance $G(T)$ of the CNT(left lead)-CNT(QD)-CNT(right lead) junction in the Kondo regime. The calculation is carried out in the weak and strong coupling regimes characterized respectively by $T \gg T_K$ and $T < T_K$. In the weak coupling regime, perturbation RG formalism is used to calculate the nonlinear conductance within the Keldysh nonequilibrium Green's function formalism. In the strong coupling regime the mean field slave boson formalism is employed, which is appropriate only within linear response.

Conductance in the weak coupling limit: Calculations of the tunneling conductance in the weak coupling regime are carried out below using the Keldysh technique in order to treat a system out of equilibrium. The required quantities to be used below are the Keldysh electron matrix Green's functions (GF) g_a for $a = lm, rm, f$ standing for left lead, right lead, and dot, respectively,

$$g_a = \begin{pmatrix} g^R_a & g^K_a \\ 0 & g^A_a \end{pmatrix}, \quad (20)$$

where the superscripts refer to retarded (R), advanced (A), and Keldysh (K) types of the GF. The explicit expressions are

$$\begin{aligned} g^R_{\alpha m} &= -g^A_{\alpha m} = -i\pi\rho_m, \\ g^K_{\alpha m}(\epsilon) &= -2i\pi\rho_m[1 - 2f(\epsilon)], \end{aligned} \quad (21)$$

$$\begin{aligned} g^{R/A}_f(\epsilon) &= \frac{1}{\epsilon - \epsilon_d \pm i\eta}, \\ g^K_f(\epsilon) &= -\frac{2i\eta[1 - 2f(\epsilon)]}{(\epsilon - \epsilon_d)^2 + \eta^2}, \end{aligned} \quad (22)$$

where $f(\epsilon)$ is the Fermi function. Within the Keldysh formalism, the tunneling current from the left to the right lead is

$$\begin{aligned} I = {} & \frac{ie}{24\hbar}\sum_{\lambda} K_{mm}(\psi^\dagger_{l\lambda}\psi_{r\lambda} - \psi^\dagger_{r\lambda}\psi_{l\lambda}) \\ & + \frac{ie}{2\hbar}\sum_{\lambda} J_{mm}Z^{\lambda\lambda}(\psi^\dagger_{l\lambda}\psi_{r\lambda} - \psi^\dagger_{r\lambda}\psi_{l\lambda}) \\ & + \frac{ie}{2\hbar}\sum_{\lambda\neq\lambda'} J_{mm'}X^{\lambda\lambda'}(\psi^\dagger_{l\lambda'}\psi_{r\lambda} - \psi^\dagger_{r\lambda'}\psi_{l\lambda}). \end{aligned} \quad (23)$$

In addition to the exchange constant j [Eq. (16)] the conductance depends also on the dimensionless parameter k, defined as [see comment after Eq. (16)]

$$k = K_{mm}\rho_m = \frac{\Gamma(2U_d - 13\epsilon_F + 13\epsilon_d)}{4\pi(\epsilon_F - \epsilon_d)(U - \epsilon_F + \epsilon_d)}. \quad (24)$$

To second order in j and k the conductance $G = \partial\langle I\rangle/\partial V$ is

$$G_2 = \frac{\pi e^2}{2N\hbar}[k^2 + (N^2 - 1)j^2], \quad (25)$$

while only j contributes to the third order correction to the conductance,

$$G_3 = \frac{(N^2 - 1)\pi e^2}{4\hbar} j^3 \ln\left[\frac{\bar{D}}{\sqrt{T^2 + (\mathrm{eV})^2}}\right]. \quad (26)$$

Due to the large prefactor and the logarithmic term, which, strictly speaking, is not small either, G_3 is not small as compared with G_2. Hence, expansion up to third order in j is inadequate. Instead, we derive an expression for the conductance in the leading logarithmic approximation using the RG equations (17).

In the following analysis we split the second order contribution to the conductance [Eq. (25)] in two parts: The first part results from exchange cotunneling, which is proportional to j^2, while the second part is due to regular cotunneling, which is proportional to k^2. The regular cotunneling contribution containing k^2 does not grow at low temperatures and/or bias, and therefore it does not contribute to the Kondo effect. The exchange cotunneling contains a term j^2 which demonstrates logarithmic enhancement of the conductance at low temperatures [see Eq. (18)] and contributes to the Kondo effect. Therefore, we single out the exchange contribution in the second order term,

$$G_2^{\text{exch}}(D) = \frac{(N^2-1)\pi e^2}{2N\hbar} j^2(D). \tag{27}$$

The condition imposing invariance of the conductance under "poor man's scaling" transformation has the form

$$\frac{\partial}{\partial \ln D}\left\{ G_2^{\text{exch}}(D) + \frac{(N^2-1)\pi e^2}{4\hbar} j^3 \times \ln\left[\frac{D}{\sqrt{T^2+(\text{eV})^2}}\right]\right\} = 0. \tag{28}$$

Within the accuracy of this equation, when differentiating the second term, we should neglect any implicit dependence on D through the couplings j. Equation (28) yields the scaling equation (17). The renormalization procedure should proceed until the bandwidth D is reduced to a quantity

$$d(T,V) = \sqrt{(\text{eV})^2 + T^2}.$$

At this point, the third order correction to the conductance vanishes and the current and conductance can be calculated in the Born approximation, as in Eq. (27) [31]. The expression for the conductance for $\text{Max}(T,|\text{eV}|) \gtrsim T_K$ is

$$G(T,V) = \frac{\pi^2 \mathcal{N} G_0}{\ln^2[d(T,V)/T_K]}, \tag{29}$$

where

$$\mathcal{N} = \frac{2(N^2-1)}{N^3}, \quad G_0 = \frac{e^2}{\pi\hbar}. \tag{30}$$

The total differential conductance (29) is displayed in Fig. 6 for $V = 0$ (zero bias differential conductance). The conductance increases when the temperature is lowered, which is typical to the standard scenario of Kondo tunneling through the tunnel junction [31]. The nonlinear conductance (29) as a function applied bias is shown in Fig. 7 for several temperatures T. The zero bias peak of the conductance is typical for the ordinary SU(2) Kondo effect.

It should be noted that the conductance (29) has a factor $\mathcal{N}$, Eq. (30), which is $\frac{3}{4}$ for $N = 2$ or $\frac{143}{864}$ for $N = 12$. In other words, as far as the conductance *in the weak coupling regime* is concerned, the main difference between the SU(12) and the

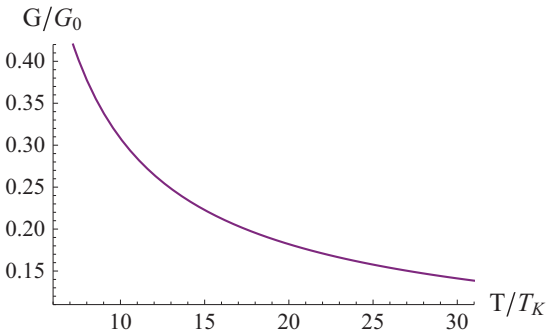

FIG. 6. (Color online) The zero bias conductance (29) as a function of temperature in the weak coupling regime.

SU(2) Kondo tunneling is the substantial difference of the corresponding Kondo temperatures (19). This similarity no longer holds in the strong coupling regime as we will now show.

Conductance in the strong coupling limit: For $T < T_K$, the mean field slave boson approximation (MFSBA) is employed to calculate the zero bias tunneling conductance. In the limit $U \to \infty$, the dot can be either empty or singly occupied. The dot electron annihilation and creation operators are written as $d_\lambda = b^\dagger f_\lambda$ and $d_\lambda^\dagger = f_\lambda^\dagger b$, where the slave fermion operators f_λ and the slave boson operator b satisfy the constraint condition

$$Q = \sum_\lambda f_\lambda^\dagger f_\lambda + b^\dagger b = 1.$$

This condition is encoded by including a Lagrange multiplier ω in the total action S. In the mean field approximation we replace the Bose operators b and $b^\dagger$ by their expectation values, $b_0 = \sqrt{\langle b^\dagger b\rangle}$. At the mean field level the constraint condition is satisfied only on the average.

The current operator reads

$$I = \frac{ieb_0}{\hbar} \sum_\lambda t_m [\psi_{l\lambda}^\dagger(0) f_\lambda - \text{H.c.}]. \tag{31}$$

It can be derived from the partition function that is formally written as

$$Z(\alpha_q) = \int D[f f^\dagger c c^\dagger] e^{-\beta S(\alpha_q)}. \tag{32}$$

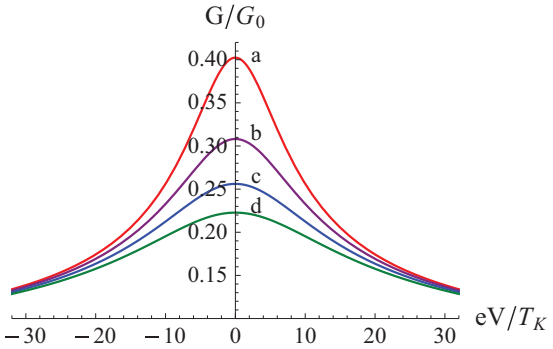

FIG. 7. (Color online) The nonlinear conductance (29) as a function of applied bias in the weak coupling regime for $T = 7.5T_K$ (curve a), $T = 10T_K$ (curve b), $T = 12.5T_K$ (curve c), and $T = 15T_K$ (curve d).

Here $S(\alpha_q)$ is the action (written explicitly below) that contains a term $\alpha_q I$ where α_q is a source field, and integration is carried out over lead $(c,c^\dagger)$ and slave fermion $(f,f^\dagger)$ fields (treated here as Grassman variables). The action is given explicitly as

$$S=\int_{-\infty}^{\infty}dt\,\mathcal{L}(t), \tag{33}$$

where $\mathcal{L}=\mathcal{L}_l+\mathcal{L}_r+\mathcal{L}_d-\mathcal{L}_t-\alpha_q I$,

$$\mathcal{L}_\alpha=\sum_{k\lambda}c^\dagger_{\alpha k\lambda}\{i\hbar\partial_t-\epsilon_{km}\}\tau^z c_{\alpha k\lambda},\quad \alpha=l,r,$$

$$\mathcal{L}_d=\sum_{\lambda}f^\dagger_{\lambda}\{i\hbar\partial_t-\epsilon_f\}\tau^z f_{\lambda},\quad \epsilon_f=\epsilon_d+\omega,$$

$$\mathcal{L}_t=\frac{b_0}{\sqrt{L_{\rm cnt}}}\sum_{\alpha k\lambda}t_m\{c^\dagger_{\alpha k\lambda}\tau^z f_\lambda+f^\dagger_\lambda\tau^z c_{\alpha k\lambda}\}.$$

The action in the MFSBA is Gaussian and depends on two real numbers, the boson field b_0 and the chemical potential (Lagrange multiplier) ω. Carrying out the integration according to Eq. (32) yields the partition function

$$\ln Z(\alpha_q)=-2\sum_m \mathrm{tr}\ln\left\{\mathcal{G}^{-1}_{fm}-\frac{e\alpha_q t_m^2 b_0^2}{\hbar}[g_{lm},\tau_x]\right\},$$

where

$$\mathcal{G}^{-1}_{fm}=g^{-1}_f-t_m^2b_0^2(g_{lm}+g_{rm}).$$

Here g_f is the GF (22) of the (noninteracting) electron in the QD with shifted energy level, $\epsilon_d\to\epsilon_f=\epsilon_d+\omega$.

The MFSBA is reliable in equilibrium, $V=0$. Therefore, we will consider below the temperature dependence of the zero bias conductance. In equilibrium, the mean field solutions for b_0 and ω minimize the free energy,

$$F=-2T\sum_{m\omega_n}\mathrm{tr}\ln\mathcal{G}^{-1}_{fm}(i\omega_n)+\omega b_0^2, \tag{34}$$

where the last term is the slave boson kinetic part of the free energy due to the constraint, and $\mathcal{G}^{-1}_{fm}(i\omega_n)$ is the Matsubara's GF. The mean field equations,

$$\begin{aligned}\frac{N}{\pi}\arctan\left(\frac{b_0^2\Gamma}{2\epsilon_f}\right)&=1-b_0^2,\\ \frac{N\Gamma}{8\pi}\ln\left(\frac{\bar{D}^2}{\left(\frac{b_0^2\Gamma}{2}\right)^2+\epsilon_f^2}\right)&=\omega\end{aligned} \tag{35}$$

are solved for ω and b_0 with the solutions,

$$\omega=-\epsilon_d+T_K\cos\left(\frac{\pi}{N}\right),\quad b_0^2=\frac{2T_K}{\Gamma}\sin\left(\frac{\pi}{N}\right),$$

where T_K is the Kondo temperature given by Eq. (19) and Γ is given in Eq. (13). The expression for the linear conductance for $T<T_K$ is now obtained as

$$G(T)=\frac{NG_0}{8T}\int\frac{d\epsilon}{\cosh^2\left(\frac{\epsilon}{2T}\right)}\frac{\left(\frac{\pi T_K}{N}\right)^2}{(\epsilon-\epsilon_f)^2+\left(\frac{\pi T_K}{N}\right)^2}, \tag{36}$$

where $\epsilon_f=T_K\cos(\pi/N)$ and G_0 is given by Eq. (30). The zero bias conductance as a function of temperature is shown in Fig. 8. It is seen that the conductance has a peak at $T\approx 0.57T_K$ due to the constraint imposed by the Friedel sum rule [29,32]. In addition to the different Kondo temperatures (19) for the SU(12) and SU(2) Kondo effects, this behavior indicates a remarkable distinction from the standard SU(2) Kondo tunneling [22]. In the latter case, the conductance is monotonically increasing towards the unitary limit as $T\to 0$. It should be noted that we define G_0 as $e^2/(6h)$ *per spin projection* [see Eq. (30)], so that the unitary limit corresponds here to $6G_0=12e^2/h$. A close inspection shows that this limit is not perfectly reached. The reason is that while the DOS has a peak that is shifted from the Fermi level by T_K, the peak of the "thermal" function $\cosh^{-2}(\epsilon/2T)$ sits right at the Fermi level. As a result, the peak of the conductance occurs at finite temperature, and its value is slightly lowered by the thermal function.

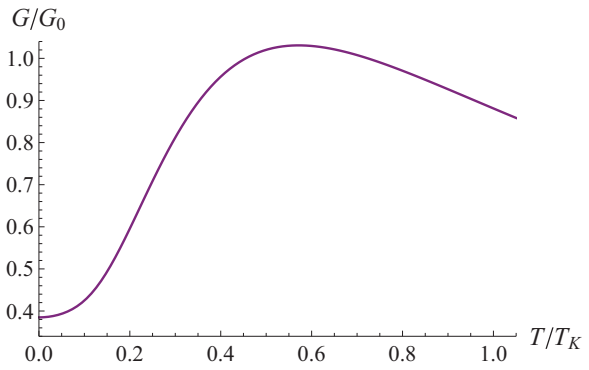

FIG. 8. (Color online) The zero bias conductance as a function of temperature in the strong coupling limit ($T<T_K$).

VII. MAGNETIC SUSCEPTIBILITY

While in bulk metals, the Kondo effect manifests itself through measurements of electrical resistivity *and* magnetic susceptibility, in quantum dots it manifests itself mainly through the properties of the conductance. Designing experiments aimed at studying magnetic response of quantum dot in the Kondo regime is rather difficult because they require an STM technique in which the tip is close to the magnetic impurity. Appropriate STM techniques have already been worked out for impurities composed of added magnetic atoms on metallic surface [33]. We are unaware of their applications in quantum dots. The discussion below is therefore motivated by our hope that measurement of magnetic response of a single magnetic impurity in quantum dot will eventually materialize.

In the CNT-CNT(QD)-CNT junction the magnetic response is encoded by the static impurity magnetic susceptibility χ of the CNT(QD) (defined explicitly below). Unlike the discussion pertaining to the conductance, there is no source-drain bias present here, and the leads just serve as a source of electron gas that acts to screen the impurity. The distinction between the present structure and that of Kondo effect in bulk CNT [7] is that here the impurity is composed of a trapped electron with a 12-fold degenerate ground state.

The Zeeman splitting $\Delta_{m\sigma}$ of electron energy levels in a carbon nanotube subject to an external magnetic field **B** depends on whether the magnetic field is parallel or perpendicular to the CNT axis (see Appendix B for details).

Explicitly,

$$\Delta_{m\sigma} = -g_{\rm orb} m \mu_B B_\parallel - g_{\rm spin} \sigma \mu_B B, \tag{37}$$

where $B = |\mathbf{B}|$, $B_\parallel$ is the component of the magnetic field parallel to the CNT axis, μ_B is the Bohr magneton, and $g_{\rm orb}$ and $g_{\rm spin}$ are orbital and spin g factors,

$$g_{\rm spin} \approx 2, \quad g_{\rm orb} = \frac{m_e v r_0}{\pi \hbar} \frac{\Delta_0}{\epsilon_F}, \tag{38}$$

where m_e is the mass of free electron.

The Zeeman splitting (37) results in an anisotropy of the magnetic susceptibility: In other words, χ is a tensor, which in the principal frame of the CNT has parallel and perpendicular components, $\chi^{\parallel}_{\rm imp}$ and $\chi^{\perp}_{\rm imp}$, responding to the magnetic field parallel or perpendicular to the CNT axis. This anisotropy is absent in the ordinary SU(2) Kondo effect, and is one of the hallmarks of a higher symmetry such as SU(12) discussed here that involves orbital symmetry.

The impurity magnetization is defined through the relation [29]

$$\mathbf{M}_{\rm imp} = g_{\rm spin}\mu_B \left\{ \left\langle \mathbf{S} + \sum_\alpha \mathbf{\Sigma}_\alpha \right\rangle - \left\langle \sum_\alpha \mathbf{\Sigma}_\alpha \right\rangle_0 \right\} + g_{\rm orb}\mu_B \mathbf{e}_x \left\{ \left\langle L^x + \sum_\alpha \Lambda^x_\alpha \right\rangle - \left\langle \sum_\alpha \Lambda^x_\alpha \right\rangle_0 \right\}, \tag{39}$$

where $\mathbf{S}$ and $\mathbf{\Sigma}_\alpha$ ($\alpha = l,r$) are, respectively, the spin operators of the dot and the lead electrons,

$$\mathbf{S} = \sum_{\lambda\lambda'} \mathbf{s}_{\sigma\sigma'} \delta_{mm'} \delta_{\xi\xi'} X^{\lambda\lambda'}, \qquad \mathbf{\Sigma}_\alpha = \sum_{k\lambda\lambda'} c^\dagger_{\alpha k\lambda} \mathbf{s}_{\sigma\sigma'} \delta_{mm'} \delta_{\xi\xi'} c_{\alpha k\lambda'}, \tag{40}$$

while L^x and Λ^x_α are, respectively, the operators of the x component of the orbital moment of the dot or the lead,

$$L^x = \sum_\lambda m X^{\lambda\lambda}, \quad \Lambda^x_\alpha = \sum_{k\lambda} m c^\dagger_{\alpha k\lambda} c_{\alpha k\lambda}. \tag{41}$$

In Eq. (39) $\langle \cdots \rangle$ indicates thermal averaging with respect to the full Hamiltonian $\tilde{H} = H_0 + H_K$ [Eqs. (9) and (15)], whereas $\langle \cdots \rangle_0$ indicates thermal averaging respect to H_0. It is reasonably assumed that electrons in the dot and the leads have the same g factors.

Susceptibility in the weak coupling regime: Using a similar analysis as for the conductance, we derive an expression for the zero-field magnetic susceptibility to second order in j,

$$\chi^{\parallel}_{\rm imp} = \left(\frac{g^2_{\rm spin}}{4} + \frac{2g^2_{\rm orb}}{3} \right) \chi(T), \tag{42}$$

$$\chi^{\perp}_{\rm imp} = \frac{g^2_{\rm spin}}{4} \chi(T), \tag{43}$$

where, to second order in j,

$$\chi(T) = \frac{\chi_0 T_K}{T} \left\{ 1 - j - \frac{Nj^2}{2} \ln\left(\frac{D}{T}\right) \right\}, \tag{44}$$

$$\chi_0 = \frac{\mu_B^2}{T_K}. \tag{45}$$

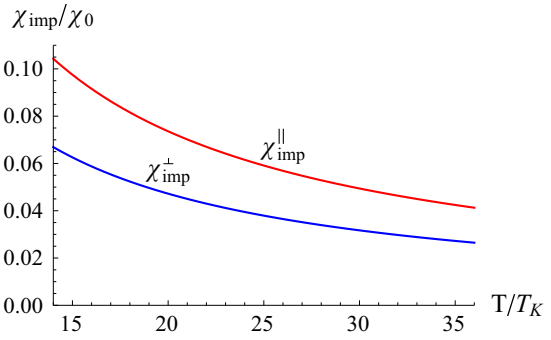

FIG. 9. (Color online) Impurity susceptibility $\chi^{\parallel}_{\rm imp}$ (red curve) and $\chi^{\perp}_{\rm imp}$ (blue curve), as a function of temperature in the weak coupling regime [Eqs. (42), (43), and (47)].

The second term on the right-hand side of Eq. (42) reflects the orbital degeneracy, and is absent in the SU(2) Kondo effect. This anisotropy of the magnetic response is one of our main results, as it constitutes an observable that is a hallmark of the SU(12) symmetry of the pertinent Kondo effect. It is compactly encoded by the temperature independent ratio

$$\frac{\chi^{\parallel}_{\rm imp}}{\chi^{\perp}_{\rm imp}} = 1 + \frac{8}{3} \frac{g^2_{\rm orb}}{g^2_{\rm spin}}. \tag{46}$$

As we shall see below, this relation holds also in the strong coupling regime $T < T_K$. It is then suspected that this result is "universal" in the sense that it holds for the crossover region $T \approx T_K$ as well. In Appendix C it is indeed shown that this ratio can be derived quite generally (in this model) by using the fluctuation-dissipation formula for the susceptibility (which relates the susceptibility to the spin correlations).

At high temperatures, the logarithmic term causes a reduction of the effective magnetic moment as compared with that for a free spin. With decreasing temperature, the second order perturbation theory becomes inadequate. In order to derive an expression for $\chi_{\rm imp}$ in the leading logarithmic approximation, we use the RG equations (17). The condition imposing the invariance of the susceptibility under the poor man's scaling transformation is

$$\frac{\chi_0 T_K}{T} \frac{\partial}{\partial \ln(D)} \left\{ 1 - j - \frac{Nj^2}{2} \ln\left(\frac{D}{T}\right) \right\} = 0.$$

Within the accuracy of this equation, when differentiating the third term, we should neglect any implicit dependence on D through the coupling j. The renormalization procedure should proceed until the bandwidth D is reduced to the temperature T. At this point, the second order of the perturbation theory vanishes and the susceptibility takes the form

$$\chi(T) = \frac{\chi_0 T_K}{T} \left\{ 1 - \frac{2}{N \ln(T/T_K)} \right\}. \tag{47}$$

The impurity susceptibility in the weak coupling regime, Eqs. (42), (43), and (47), is shown in Fig. 9.

Susceptibility in the strong coupling regime: For $T < T_K$, the magnetic susceptibility can be calculated in the framework of the MFSBA. For this purpose, we take into account the dependence of the right-hand side of Eq. (34) for the free energy on the external magnetic field $\mathbf{B}$. Because

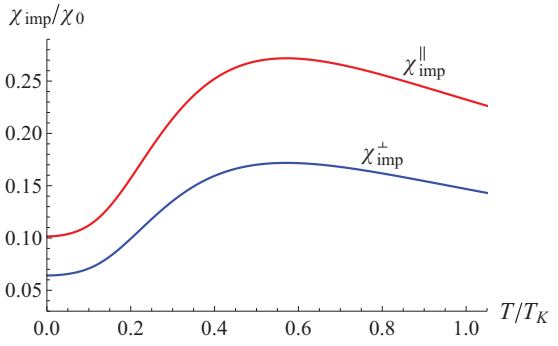

FIG. 10. (Color online) Impurity susceptibility $\chi^{\parallel}_{\rm imp}$ (red curve) and $\chi^{\perp}_{\rm imp}$ (blue curve) as a function of temperature in the strong coupling regime [Eqs. (42), (43), and (48)].

the susceptibility tensor is diagonal, we may write $\chi^{i}_{\rm imp} = -[\partial^2 F(\mathbf{B})/\partial B_i^2]_{\mathbf{B}=0}$, where $i = \parallel, \perp$. Thereby we get the zero field susceptibility $\chi^{\parallel}_{\rm imp}$ or $\chi^{\perp}_{\rm imp}$. Explicitly, for magnetic field parallel or perpendicular to the CNT axis, the susceptibility is given by Eq. (42) or (43), with $\chi(T)$ given by

$$\chi(T) = \frac{\chi_0}{4T}\int \frac{d\epsilon}{\cosh^2\left(\frac{\epsilon}{2T}\right)} \frac{\left(\frac{T_K}{N}\right)^2}{(\epsilon + T_K)^2 + \left(\frac{\pi T_K}{N}\right)^2}. \tag{48}$$

The magnetic susceptibilities in the strong coupling regime are shown in Fig. 10. They display a peak at finite temperature, commensurate with the constraint imposed by the Friedel sum rule [29,32,34].

VIII. CONCLUSIONS

Whereas the theoretical framework of the Coqblin-Schrieffer model is intensively studied, the present work focuses on one of its special facets that is less explored, namely, its possible realization in a transport device with a Dirac spectrum and peculiar DOS. We substantiate the possibility of tuning a metallic CNT into a tunnel junction consisting of two CNT metallic leads and a CNT(QD). The spin, isospin (valley), and orbital degeneracy of the CNT(QD) energy spectrum gives rise to the Kondo effect with SU(12) dynamical symmetry. The high symmetry of the CNT(QD) leads to an enhanced Kondo temperature. The conductance through the junction is evaluated using Keldysh technique. Renormalization group analysis is performed in the weak coupling regime ($T \gg T_K$) while the MFSBA is used at the strong coupling regime $T < T_K$. In the weak coupling regime, the behavior of $G(T)$ as function of temperature for the SU(12) Kondo effect is qualitatively the same as that for the ordinary SU(2) Kondo effect, and the main difference is that $T_K[\mathrm{SU}(12)] \gg T_K[\mathrm{SU}(2)]$. In the strong coupling regime the situation is different. Due the constraints imposed by the Friedel sum rule, the conductance has a peak at finite temperature that becomes sharper the higher is N. This distinction of the conductance between SU(2) and SU(12) Kondo effect in quantum dot should be experimentally observable.

The magnetic response exposes yet another remarkable distinction between the SU(12) and the SU(2) Kondo effects. For the SU(12) Kondo effect, the response is anisotropic and the susceptibility is a tensor. It has two components, $\chi^{\parallel}_{\rm imp}$ and $\chi^{\perp}_{\rm imp}$, according to whether the magnetic field is along the CNT axis or perpendicular to it. Moreover, the ratio $\chi^{\parallel}_{\rm imp}/\chi^{\perp}_{\rm imp} = 1 + 8g^2_{\rm orb}/(3g^2_{\rm spin})$ depends only on the orbital and spin g factors. This result is demonstrated in the weak coupling regime based on RG calculations and in the strong coupling regime based on the MFSBA. A proof that this result is true in every order of perturbation theory is derived in Appendix C employing the fluctuation-dissipation theorem. An experimental search for such anisotropy would constitute a confirmation of this unusual Kondo effect, but as was pointed out earlier, observing magnetic response of a single impurity is quite difficult.

The Kondo physics in systems with Dirac spectrum proves to be rather rich. While the Kondo effect in bulk graphene reveals peculiar equilibrium properties such as the existence of two distinct classes of Kondo quantum critical points [35], analysis of nonequilibrium transport in correlated CNT(left lead)-CNT(QD)-CNT(right lead) junction reveals another facet, namely, Kondo tunneling with an SU(12) dynamical symmetry.

ACKNOWLEDGMENTS

We would like to thank Natan Andrei for stimulating discussions. Correspondence with George Martins is highly appreciated. This research was supported by the Israeli Science Foundation for supporting our research under Grants 1173/08 and 400/2012.

APPENDIX A: WAVE FUNCTIONS OF CNT QUANTUM DOT

For electrons in CNT(QD), the single electron wave functions and the corresponding energy spectrum are derived from the Dirac equation (4). The solution $\Phi_{mn}(x,\phi)$ of the Dirac equation is written as

$$\Phi_{mn}(x,\phi) = \begin{cases} \Phi^{(1)}_{mn}(x)e^{im\phi} & \text{if} \quad |x| < h, \\ \Phi^{(2)}_{mn}(x)e^{im\phi} & \text{if} \quad x > h, \\ \Phi^{(3)}_{mn}(x)e^{im\phi} & \text{if} \quad x < -h, \end{cases} \tag{A1}$$

where $m = 0, \pm1, \pm2, \ldots$ is a magnetic quantum number, $n = 0,1,2,\ldots$ is a radial quantum number.

The function $\Phi^{(1)}_{mn}(x)$ is given by

$$\Phi^{(1)}_{mn}(x) = \frac{A_{mn}}{\sqrt{\epsilon}}\left\{\chi^{(1)}_{\uparrow}\sqrt{\epsilon + M_m}\cos\left(k_x x + \frac{n\pi}{2}\right) + \chi^{(1)}_{\downarrow}\sqrt{\epsilon - M_m}\sin\left(k_x x + \frac{n\pi}{2}\right)\right\}, \tag{A2}$$

where M_m and M_0 are defined through the relations

$$\hbar v k_x = \sqrt{\epsilon^2 - M_m^2}, \quad M_m = \sqrt{M_0^2 + m^2\Delta_0^2}.$$

The expressions for the spinors $\chi^{(1)}_{\sigma}$ and $\chi^{(2)}_{\sigma}$ (to be used later) are given in Eq. (8).

The function $\Phi^{(1)}_{m}(x)$ has the following symmetry:

$$\hat{M}_m \Phi^{(1)}_m(-x) = (-1)^n M_m \Phi^{(1)}_m(x).$$

Similarly, the function $\Phi^{(2)}_m(x)$ (for $x > h$) reads

$$\Phi^{(2)}_{mn}(x) = \frac{B_m e^{-\kappa(x-h)}}{\sqrt{2N_m}}\left\{\chi^{(2)}_\uparrow\sqrt{N_m+\epsilon}+\chi^{(2)}_\downarrow\sqrt{N_m-\epsilon}\right\}, \tag{A3}$$

where N_m and N_0 are defined through

$$\hbar v\kappa = \sqrt{N_m^2-\epsilon^2}, \quad N_m = \sqrt{N_0^2+m^2\Delta_0^2}.$$

Finally, the function $\Phi^{(3)}_{mn}(x)$ (for $x < -h$) is

$$\Phi^{(3)}_{mn}(x) = \frac{(-1)^n}{N_m}\hat{N}_m\Phi^{(2)}_{mn}(-x).$$

Applying the continuity condition for $\Phi_{mn}(x,\phi)$, Eq. (A1) at the points $x = \pm h$, we obtain the set of equations,

$$A_{mn}\sqrt{\epsilon+M_m}\cos\left(k_x h+\frac{n\pi}{2}\right) = B_{mn}\mathcal{F}_\uparrow(\epsilon), \tag{A4a}$$

$$A_{mn}\sqrt{\epsilon-M_m}\sin\left(k_x h+\frac{n\pi}{2}\right) = B_{mn}\mathcal{F}_\downarrow(\epsilon), \tag{A4b}$$

where $\mathcal{F}_\sigma(\epsilon)$ is given by Eq. (7).

The set of equations (A4) has nontrivial solutions when its determinant vanishes. This condition gives us Eq. (6) for the energy levels in the quantum dot.

APPENDIX B: MAGNETIZATION OF THE TUNNEL JUNCTION

It order to describe electronic properties of a carbon nanotube in an external magnetic field $\mathbf{B}$, we should add to the CNT Hamiltonian the term H_B describing spin-Zeeman splitting,

$$H_{\rm spin} = -g_{\rm spin}\mu_B(\mathbf{s}\cdot\mathbf{B}), \tag{B1}$$

and replace the wave vector $\mathbf{k}$ by the operator $\mathbf{k}'$ [18,19],

$$\mathbf{k}\to\mathbf{k}' = -i\nabla - \frac{e}{\hbar c}\mathbf{A}.$$

Here $\mathbf{s}$ is a vector of the spin operators, $\mathbf{A}$ is a vector potential, $\mathbf{B} = \nabla\times\mathbf{A}$. Then the motion of electron in a CNT with the wave vector close to the $\mathbf{K}$ point of the first Brillouin zone can be described by the Hamiltonian,

$$H = \hbar v\left(\mathbf{k}-\frac{e}{\hbar c}\mathbf{A}\right)\boldsymbol{\tau}+\Delta_g\tau_z+H_{\rm spin}. \tag{B2}$$

Here we use use the cylindrical system of coordinates where $\mathbf{k} = (k_x,k_y)$ with $k_x = -i\partial_x$ and $k_y = -\frac{i}{r_0}\partial_\phi$. The Hamiltonian for the motion of electron with the wave vector near $\mathbf{K}'$ point can be obtained from Eq. (B2) just by replacing $k_y\to -k_y$.

In what follows, we will calculate Zeeman splitting for the magnetic field parallel and perpendicular to the CNT axis.

Magnetic field parallel to the CNT axis: When the magnetic field is parallel to the CNT axis, $\mathbf{B}_\parallel = B\mathbf{e}_x$, the vector potential can be written as

$$\mathbf{A}_\parallel = \frac{Br}{2}\mathbf{e}_\phi. \tag{B3}$$

The eigenfunction of the Hamiltonian (B2) is

$$|\Psi^\parallel_{skm\sigma}(\varphi)\rangle = |\chi_\sigma\rangle\otimes|\psi_{skm}(\varphi)\rangle, \tag{B4}$$

where $\varphi = \pi Br_0^2$ is the magnetic flux through the cross section of the CNT. Here $|\chi_\sigma\rangle$ is a spin wave function of electron with spin parallel or antiparallel to the magnetic field,

$$|\chi_\uparrow\rangle = \begin{pmatrix}1\\0\end{pmatrix}, \quad |\chi_\downarrow\rangle = \begin{pmatrix}0\\1\end{pmatrix}. \tag{B5}$$

$|\psi_{skm}(\varphi)\rangle$ is the spatial wave function of electron in the conduction ($s = +1$) or valence ($s = -1$) band with orbital quantum number m ($m = 0,\pm1$), and wave number k,

$$|\psi_{skm}(\varphi)\rangle = \frac{e^{ikx+im\phi}}{\sqrt{4\pi L}}\begin{pmatrix}sb_{km}(\varphi)\\1\end{pmatrix},$$
$$b_{km}(\varphi) = \frac{\kappa_m(\varphi)-ik}{\sqrt{\kappa_m^2(\varphi)+k^2}}, \tag{B6}$$
$$\kappa_m(\varphi) = \frac{m-\varphi}{r_0}.$$

The corresponding energy is

$$\tilde{\varepsilon}_{sk\lambda} = s\sqrt{(\hbar vk)^2+(m-\varphi)^2\Delta_0^2+\Delta_g^2}-2\sigma\mu_B B. \tag{B7}$$

For weak magnetic fields ($\varphi\ll 1$), $\varepsilon_{sk\lambda}$ can be expanded to linear with B correction,

$$\tilde{\varepsilon}_{sk\lambda} = \varepsilon_{skm}-\frac{\Delta_0^2 m\varphi}{\varepsilon_{skm}}-2\sigma\mu_B B+O(\varphi^2),$$
$$\varepsilon_{skm} = s\sqrt{(\hbar vk)^2+m^2\Delta_0^2+\Delta_g^2}.$$

Then for ε_{skm} close to the Fermi level, we get Eq. (37).

Then the magnetization (39) in linear with B approximation is

$$M^x_{\rm imp} = g^2_{\rm spin}\mu_B^2 B\left\{\langle(\tilde{\Sigma}^x)^2\rangle-\left\langle\sum_\alpha\left(\Sigma^x_\alpha\right)^2\right\rangle_0\right\}$$
$$+g^2_{\rm orb}\mu_B^2 B\left\{\langle(\tilde{\Lambda}^x)^2\rangle-\left\langle\sum_\alpha\left(\Lambda^x_\alpha\right)^2\right\rangle_0\right\}, \tag{B8}$$

where $\tilde{\boldsymbol{\Sigma}} = (\tilde{\Sigma}^x,\tilde{\Sigma}^y,\tilde{\Sigma}^z)$ is the total spin of the tunnel junction,

$$\tilde{\boldsymbol{\Sigma}} = \mathbf{S}+\sum_\alpha\boldsymbol{\Sigma}_\alpha, \tag{B9}$$

$\tilde{\Lambda}^x$ is the orbital momentum of the total system,

$$\tilde{\Lambda}^x = L^x+\sum_\alpha\Lambda^x_\alpha. \tag{B10}$$

Magnetic field perpendicular to the CNT axis: Let us consider now the magnetic field perpendicular to the CNT axis. For definiteness, we take $\mathbf{B}_\perp = B[\mathbf{e}_r\cos\phi-\mathbf{e}_\phi\sin\phi]$, so that $\mathbf{A}_\perp = Br\sin\phi\mathbf{e}_x$. Then the Hamiltonian (B2) takes the form

$$H = H_0+H_{\rm spin}+H_{\rm orb}, \quad H_0 = \hbar v\boldsymbol{\tau}\cdot\mathbf{k}+\Delta_g\tau_z, \tag{B11}$$

where $H_{\rm spin}$ is given by Eq. (B1),

$$H_{\rm orb} = -\frac{\Delta_0 r_0^2}{l_B^2}\sin\phi\tau_x, \tag{B12}$$

l_B is the magnetic length given by

$$l_B = \sqrt{\frac{c\hbar}{Be}}. \tag{B13}$$

When $l_B \gg r_0$, the field can be regarded as a small perturbation.

The eigenfunction of the Hamiltonian $H_0 + H_{\rm spin}$ are $|\chi_\sigma\rangle \otimes |\psi_{skm}\rangle$, where $|\chi_\sigma\rangle$ describes the quantum state with the spin parallel or antiparallel to the magnetic field $\mathbf{B}$, $|\psi_{skm}\rangle$ is the spatial wave function of electron with wave number k, orbital number m in the conduction or valence band, $s = \pm 1$.

In order to estimate the contribution of $H_{\rm orb}$, we note that the nontrivial matrix elements of $H_{\rm orb}$ are

$$\langle\psi_{skm}|H_{\rm orb}|\psi_{skm+1}\rangle, \quad \langle\psi_{skm+1}|H_{\rm orb}|\psi_{skm}\rangle,$$

i.e., $H_{\rm orb}$ change the orbital quantum number by ± 1 keeping the other quantum numbers (wave number, band index, spin, etc.) unchanged. The quantum transitions from the state $|\psi_{skm}\rangle$ to the state $|\psi_{skm+1}\rangle$ costs the energy $\varepsilon_{skm+1} - \varepsilon_{skm} \sim \Delta_0$. As a result, for low magnetic fields ($l_B \gg r_0$), corrections of $H_{\rm orb}$ to the energy spectrum is of order $l_B^{-4} \sim B^2$ and the energy dispersion in linear with B approximation is given by Eq. (37).

The magnetization (39) in linear with B approximation is

$$M^{\perp}_{\rm imp} = g^2_{\rm spin}\mu_B^2 B \left\{ \left\langle \left(\tilde{\Sigma}^y_\alpha\right)^2 \right\rangle - \left\langle \sum_\alpha \left(\Sigma^y_\alpha\right)^2 \right\rangle_0 \right\}, \tag{B14}$$

where we take the y component of the spin operators for definiteness, $\tilde{\Sigma}^y$ is given by Eq. (B9).

APPENDIX C: MAGNETIC SUSCEPTIBILITY OF CNT QD: FLUCTUATION-DISSIPATION THEOREM

In this section we derive the universal relation (46) using the fluctuation dissipation theorem.

1. Magnetic susceptibility

According to the fluctuation-dissipative theorem, the tensor of the magnetic susceptibility of the quantum dot is defined as

$$\chi_{ij} = -\frac{\partial^2 F}{\partial B_i \partial B_j} = \frac{1}{T}\left\{\langle m_i m_j\rangle - \langle m_i\rangle\langle m_j\rangle - \left\langle m_i^{(0)} m_j^{(0)}\right\rangle_0 + \left\langle m_i^{(0)}\right\rangle_0 \left\langle m_j^{(0)}\right\rangle_0\right\}. \tag{C1}$$

Here $\langle\cdots\rangle$ denotes the thermal average with respect to the Hamiltonian of interacting quantum dot and leads, $\langle\cdots\rangle_0$ is the average with respect to the Hamiltonian of the isolated leads. $i,j = x,y,z$ are Cartesian indices, $\mathbf{m} = (m_x, m_y, m_z)$ is magnetic momentum of the quantum dot and the lead, $\mathbf{m}^{(0)} = (m_x^{(0)}, m_y^{(0)}, m_z^{(0)})$ is magnetic moment of isolated leads,

$$\mathbf{m} = g_{\rm spin}\mu_B \left\{\mathbf{S} + \sum_\alpha \mathbf{\Sigma}_\alpha\right\} + g_{\rm orb}\mu_B \mathbf{e}_x \left\{L^x + \sum_\alpha \Lambda^x_\alpha\right\}, \tag{C2}$$

$$\mathbf{m}^{(0)} = g_{\rm spin}\mu_B \sum_\alpha \mathbf{\Sigma}_\alpha + g_{\rm orb}\mu_B \mathbf{e}_x \sum_\alpha \Lambda^x_\alpha, \tag{C3}$$

where the spin operators of the dot and the lead electrons ($\mathbf{S}$ and $\mathbf{\Sigma}_\alpha$, $\alpha = l,r$) are given by Eq. (40), while the operators of the x component of the orbital moment of the dot and the lead (L^x and Λ^x_α, $\alpha = l,r$) are given by Eq. (41). The Hubbard operator $X^{\lambda\lambda'} = |\lambda\rangle\langle\lambda'|$ is defined after Eq. (15). It is reasonably assumed that electrons in the dot and the leads have the same g factors.

We choose the set of coordinates in such a way that the x axis is parallel to the CNT axis, whereas the y and z axes are perpendicular. In this set of coordinates, the tensor of the susceptibility is diagonal,

$$\hat{\chi} = \begin{pmatrix} \chi_\parallel & 0 & 0 \\ 0 & \chi_\perp & 0 \\ 0 & 0 & \chi_\perp \end{pmatrix}.$$

We will prove that the zero-field susceptibilities satisfy the ratio

$$\frac{\chi_\parallel}{\chi_\perp} = 1 + \frac{8}{3}\frac{g^2_{\rm orb}}{g^2_{\rm spin}}. \tag{C4}$$

For this purpose, we note the following: The Kondo Hamiltonian (15) describes the cotunneling process such that an electron with the quantum number λ (the spin σ, the orbital quantum number m, and the valley number ξ) exits from the dot to the lead and another electron with the quantum number λ' (the spin σ', the orbital quantum number m', and the valley number ξ') enters the quantum dot from the lead. That mean that the total spin and the total orbital momentum of the lead and the quantum dot are the good quantum numbers.

Proof. Let us consider first $\chi_\perp$,

$$\chi_\perp = \frac{g^2_{\rm spin}\mu_B^2}{T}\left\{\left\langle S^z S^z + 2\sum_\alpha S^z\Sigma^z_\alpha + \sum_{\alpha\alpha'}\Sigma^z_\alpha\Sigma^z_{\alpha'}\right\rangle - \sum_{\alpha\alpha'}\left\langle\Sigma^z_\alpha\Sigma^z_{\alpha'}\right\rangle_0\right\}. \tag{C5}$$

The total Hamiltonian satisfies the SU(12) symmetry, so that we can apply such a unitary transformation that make the spin operators S^z and Σ^z_α become diagonal. This unitary transformation does not change the thermal average of the spin operators, so that $\chi_\perp$ (C5) is

$$\chi_\perp = \frac{g^2_{\rm spin}\mu_B^2}{T}\sum_{\lambda\lambda'}\frac{\sigma\sigma'}{4}\left\{\left\langle X^{\lambda\lambda}\delta_{\lambda\lambda'} + 2\sum_{\alpha k} c^\dagger_{\alpha k\lambda}c_{\alpha k\lambda}X^{\lambda'\lambda'} + \sum_{\alpha\alpha' kk'} c^\dagger_{\alpha k\lambda}c_{\alpha k\lambda}c^\dagger_{\alpha' k'\lambda'}c_{\alpha' k'\lambda'}\right\rangle - \sum_{\alpha\alpha' kk'}\langle c^\dagger_{\alpha k\lambda}c_{\alpha k\lambda}c^\dagger_{\alpha' k'\lambda'}c_{\alpha' k'\lambda'}\rangle_0\right\}. \tag{C6}$$

We will estimate each term on the right-hand side of Eq. (C6) in turn. The first term gives

$$X_{dd} = \sum_\lambda \frac{\sigma^2}{4}\langle X^{\lambda\lambda}\rangle = \frac{1}{4}, \tag{C7a}$$

where $\langle X^{\lambda\lambda}\rangle = \frac{1}{N}$ ($N = 12$) does not depend on the quantum number λ.

The second term on the right-hand side of Eq. (C6) is

$$X_{d\alpha} = \sum_{k\lambda\lambda'} \frac{\sigma\sigma'}{2} \langle c^\dagger_{\alpha k\lambda} c_{\alpha k\lambda} X^{\lambda'\lambda'} \rangle .$$

The antiferromagnetic Kondo interaction makes the difference between the two-particle states with parallel and antiparallel spins, therefore $X_{d\alpha}$ is not zero. In Appendix C 2 it is a proof that

$$P_1 = \langle c^\dagger_{\alpha k\lambda} c_{\alpha k\lambda} X^{\lambda\lambda} \rangle \tag{C7b}$$

does not depend on λ, whereas

$$P_2 = \langle c^\dagger_{\alpha k\lambda} c_{\alpha k\lambda} X^{\lambda'\lambda'} \rangle \tag{C7c}$$

does not depend on λ and λ' (just we should keep $\lambda \neq \lambda'$). Using these equalities, we can write

$$X_{d\alpha} = \frac{N}{2}\{P_1 - P_2\}. \tag{C7d}$$

The third term on the right-hand side of Eq. (C6) is

$$X_{\alpha\alpha'} = \sum_{kk'\lambda\lambda'} \frac{\sigma\sigma'}{4} \langle c^\dagger_{\alpha k\lambda} c_{\alpha k\lambda} c^\dagger_{\alpha' k'\lambda'} c_{\alpha' k'\lambda'} \rangle .$$

$X_{\alpha\alpha'}$ can be estimated similarly to $X_{d\alpha}$. The exchange interaction between the leads and the dot generates an effective interaction between electrons in the leads. As a result, the expectation value $\langle c^\dagger_{\alpha k\lambda} c_{\alpha k\lambda} c^\dagger_{\alpha' k'\lambda'} c_{\alpha' k'\lambda'} \rangle$ depends on either λ is equal to λ' or not. Defining $K_{1\alpha\alpha'}$ and $K_{2\alpha\alpha'}$,

$$\begin{aligned} K_{1\alpha\alpha'} &= \sum_{kk'} \langle c^\dagger_{\alpha k\lambda} c_{\alpha k\lambda} c^\dagger_{\alpha' k\lambda} c_{\alpha' k\lambda} \rangle \\ &\quad - \sum_{kk'} \langle c^\dagger_{\alpha k\lambda} c_{\alpha k\lambda} c^\dagger_{\alpha' k\lambda} c_{\alpha' k\lambda} \rangle_0 , \\ K_{2\alpha\alpha'} &= \sum_{kk'} \langle c^\dagger_{\alpha k\lambda} c_{\alpha k\lambda} c^\dagger_{\alpha' k'\lambda'} c_{\alpha' k'\lambda'} \rangle \\ &\quad - \sum_{kk'} \langle c^\dagger_{\alpha k\lambda} c_{\alpha k\lambda} c^\dagger_{\alpha' k'\lambda'} c_{\alpha' k'\lambda'} \rangle_0 , \quad \lambda \neq \lambda' \end{aligned} \tag{C7e}$$

($K_{1\alpha\alpha'}$ and $K_{2\alpha\alpha'}$ do not depend on λ [36]), we get

$$X_{\alpha\alpha'} = \frac{N}{4}\{K_{1\alpha\alpha'} - K_{2\alpha\alpha'}\}. \tag{C7f}$$

With Eqs. (C7a), (C7d), and (C7f), the susceptibility $\chi_\perp$ takes the form

$$\begin{aligned} \chi_\perp = \frac{g^2_{\rm spin}\mu_B^2}{4T} \Big\{ & 1 + 4N(P_1 - P_2) \\ & + N \sum_{\alpha\alpha'} (K_{1\alpha\alpha'} - K_{2\alpha\alpha'}) \Big\} . \end{aligned} \tag{C8}$$

Now consider $\chi_\parallel$,

$$\begin{aligned} \chi_\parallel = {} & \frac{g^2_{\rm spin}\mu_B^2}{T} \left\{ \left\langle S^x S^x + 2\sum_\alpha S^x \Sigma^x_\alpha + \sum_{\alpha\alpha'} \Sigma^x_\alpha \Sigma^x_{\alpha'} \right\rangle \right. \\ & \left. - \sum_{\alpha\alpha'} \langle \Sigma^x_\alpha \Sigma^x_{\alpha'} \rangle_0 \right\} \\ & + \frac{g_{\rm spin} g_{\rm orb} \mu_B^2}{T} \left\{ \left\langle S^x L^x + \sum_\alpha \left(S^x \Lambda^x_\alpha + L^x \Sigma^x_\alpha \right) \right. \right. \\ & \left. + \sum_{\alpha\alpha'} \Sigma^x_\alpha \Lambda^x_{\alpha'} \right\rangle - \sum_{\alpha\alpha'} \langle \Sigma^x_\alpha \Lambda^x_{\alpha'} \rangle_0 \Big\} \\ & + \frac{g^2_{\rm orb}\mu_B^2}{T} \left\{ \left\langle L^x L^x + 2\sum_\alpha L^x \Lambda^x_\alpha \right. \right. \\ & \left. \left. + \sum_{\alpha\alpha'} \Lambda^x_\alpha \Lambda^x_{\alpha'} \right\rangle - \sum_{\alpha\alpha'} \langle \Lambda^x_\alpha \Lambda^x_{\alpha'} \rangle_0 \right\} . \end{aligned} \tag{C9}$$

The right-hand side of Eq. (C9) consists of three blocks of terms consisting of the spin-spin, spin-orbital, and orbital-orbital correlation functions. The Kondo Hamiltonian (15) does not contain the spin-orbital interactions, so that the spin-orbital correlation functions are zero. In order to derive the spin-spin part of $\chi_\parallel$, we apply the unitary transformations to make the spins S^x and Σ^x diagonal. It is easy to see that the spin part of $\chi_\parallel$ gives Eq. (C8). Consider now the last block of terms coming from the orbital-orbital correlations. Applying the unitary transformations to make the orbital moments L^x and Λ^x_α diagonal, we can write the orbital moment contribution to $\chi_\parallel$ as

$$\begin{aligned} \chi^{\rm orb}_\parallel = {} & \frac{g^2_{\rm orb}\mu_B^2}{T} \sum_{mm'} mm' \left\{ \left\langle X^{mm}\delta_{mm'} + 2\sum_{\alpha k} c^\dagger_{\alpha k\lambda} c_{\alpha k\lambda} X^{\lambda'\lambda'} \right. \right. \\ & \left. + \sum_{\alpha\alpha' kk'} c^\dagger_{\alpha k\lambda} c_{\alpha k\lambda} c^\dagger_{\alpha' k'\lambda'} c_{\alpha' k'\lambda'} \right\rangle \\ & \left. - \sum_{\alpha\alpha' kk'} \langle c^\dagger_{\alpha k\lambda} c_{\alpha k\lambda} c^\dagger_{\alpha' k'\lambda'} c_{\alpha' k'\lambda'} \rangle_0 \right\} . \end{aligned} \tag{C10}$$

The right-hand side of Eq. (C10) consists of the terms coming from the dot-dot, dot-lead, and lead-lead correlations. We will consider all of them in turn.

The dot-dot correlation is

$$O_{dd} = \sum_\lambda m^2 \langle X^{\lambda\lambda} \rangle = \frac{2}{3} = \frac{8}{3} X_{dd} . \tag{C11a}$$

The dot-lead correlation is

$$O_{d\alpha} = 2\sum_{k\lambda\lambda'} mm' \langle c^\dagger_{\alpha k\lambda} c_{\alpha k\lambda} X^{\lambda'\lambda'} \rangle .$$

Similarly to $X_{d\alpha}$, $O_{d\alpha}$ can be expressed in terms of P_1 and P_2 [Eqs. (C7b) and (C7c)] as

$$O_{d\alpha} = 16(P_1 - P_2) = \tfrac{8}{3} X_{d\alpha} . \tag{C11b}$$

Finally, the lead-lead correlation gives

$$O_{\alpha\alpha'} = \sum_{kk'\lambda\lambda'} mm' \langle c^\dagger_{\alpha k\lambda} c_{\alpha k\lambda} c^\dagger_{\alpha' k'\lambda'} c_{\alpha' k'\lambda'} \rangle .$$

Similarly to $X_{\alpha\alpha'}$, $O_{\alpha\alpha'}$ can be expressed in terms of $K_{1\alpha\alpha'}$ and $K_{2\alpha\alpha'}$ [Eqs. (C7e) and (C7e)] as

$$O_{\alpha\alpha'} = 8(K_{1\alpha\alpha'} - K_{2\alpha\alpha'}) = \tfrac{8}{3} X_{\alpha\alpha'}. \tag{C11c}$$

Combining Eqs. (C10) and (C11), we get $\chi_\parallel$ in the form

$$\chi_\parallel = \frac{\mu_B^2}{T} \left(\frac{g_{\rm spin}^2}{4} + \frac{2 g_{\rm spin}^2}{3} \right) \times \left\{ 1 + 4N(P_1 - P_2) + N \sum_{\alpha\alpha'} (K_{1\alpha\alpha'} - K_{2\alpha\alpha'}) \right\}. \tag{C12}$$

Equations (C12) and (C8) prove Eq. (C4).

2. Proof of Eqs. (C7b) and (C7c)

In order to prove Eq. (C7b), we prove that two expected values, $G_{\lambda\lambda}$ and $G_{\lambda'\lambda'}$, are equal to one another,

$$G_{\lambda\lambda} = \langle c^\dagger_{\alpha k\lambda} c_{\alpha k\lambda} X^{\lambda\lambda} \rangle, \quad G_{\lambda'\lambda'} = \langle c^\dagger_{\alpha k\lambda'} c_{\alpha k\lambda'} X^{\lambda'\lambda'} \rangle, \tag{C13}$$

where $\lambda \neq \lambda'$. Let us, for brevity, enumerate the quantum states of the quantum dot in such a way that $\lambda = 1$ and $\lambda' = 2$. The expected value $G_{\lambda'\lambda'}$ is invariant with respect to any unitary transformations,

$$c_{\alpha k\lambda'} \to \sum_{\lambda''} U_{\lambda'\lambda''} c_{\alpha k\lambda''},$$
$$c^\dagger_{\alpha k\lambda'} \to \sum_{\lambda''} c^\dagger_{\alpha k\lambda''} U_{\lambda''\lambda'},$$
$$X^{\lambda'\lambda'} \to \sum_{\lambda''\lambda'''} U^{\lambda'\lambda''} X^{\lambda''\lambda'''} U^{\lambda'''\lambda'},$$

where $U_{\lambda'\lambda''}$ is a unitary $N \times N$ matrix. In particular, it is invariant with respect to the transformation given by the matrix,

$$U = \begin{pmatrix} 0 & 1 & 0 \\ 1 & 0 & 0 \\ 0 & 0 & \hat{I}_{10} \end{pmatrix},$$

where $\hat{I}_{10}$ is the 10×10 identity matrix. Applying this transformation to the expected value $G_{\lambda'\lambda'}$, we get the expected value $G_{\lambda\lambda}$, so that $G_{\lambda\lambda} = G_{\lambda'\lambda'}$.

In order to prove Eq. (C7c), we consider two expected values, $G_{\lambda\lambda'}$ and $G_{\lambda\lambda''}$, are equal to one another,

$$G_{\lambda\lambda'} = \langle c^\dagger_{\alpha k\lambda} c_{\alpha k\lambda} X^{\lambda'\lambda'} \rangle,$$
$$G_{\lambda\lambda''} = \langle c^\dagger_{\alpha k\lambda} c_{\alpha k\lambda} X^{\lambda''\lambda''} \rangle, \tag{C14}$$

where $\lambda \neq \lambda'$, $\lambda \neq \lambda''$, and $\lambda' \neq \lambda''$. Let us, for brevity, enumerate the quantum states of the quantum dot in such a way that $\lambda = 1$, $\lambda' = 2$, and $\lambda'' = 3$. The expected value $G_{\lambda\lambda''}$ is invariant with respect to any unitary transformations,

$$c_{\alpha k\lambda} \to \sum_{\lambda_1} U_{\lambda\lambda_1} c_{\alpha k\lambda_1},$$
$$c^\dagger_{\alpha k\lambda} \to \sum_{\lambda_1} c^\dagger_{\alpha k\lambda_1} U_{\lambda_1\lambda},$$
$$X^{\lambda''\lambda''} \to \sum_{\lambda_1\lambda_2} U^{\lambda''\lambda_1} X^{\lambda_1\lambda_2} U^{\lambda_2\lambda''},$$

where $U_{\lambda'\lambda''}$ is a unitary $N \times N$ matrix. In particular, it is invariant with respect to the transformation given by the matrix

$$U = \begin{pmatrix} 1 & 0 & 0 & 0 \\ 0 & 0 & 1 & 0 \\ 0 & 1 & 0 & 0 \\ 0 & 0 & 0 & \hat{I}_9 \end{pmatrix},$$

where $\hat{I}_9$ is the 9×9 identity matrix. Applying this transformation to the expected value $G_{\lambda\lambda''}$, we get the expected value $G_{\lambda\lambda'}$, so that $G_{\lambda\lambda''} = G_{\lambda\lambda'}$.

[1] J. S. Lim, R. Lopez, G. L. Giorgi, and D. Sanchez, Phys. Rev. B **83**, 155325 (2011).
[2] M. R. Galpin, F. W. Jayatilaka, D. E. Logan, and F. B. Anders, Phys. Rev. B **81**, 075437 (2010).
[3] C. Mora, P. Vitushinsky, X. Leyronas, A. A. Clerk, and K. Le Hur, Phys. Rev. B **80**, 155322 (2009).
[4] J. S. Lim, M.-S. Choi, M. Y. Choi, R. Lopez, and R. Aguado, Phys. Rev. B **74**, 205119 (2006).
[5] C. A. Büsser and G. B. Martins, Phys. Rev. B **75**, 045406 (2007).
[6] M. Mizuno, E. H. Kim, and G. B. Martins, J. Phys.: Condens. Matter **21**, 292203 (2009).
[7] D. H. Cobden and P. E. Lindelof, Nature (London) **408**, 342 (2000).
[8] J. Basset, A. Yu. Kasumov, C. P. Moca, G. Zaránd, P. Simon, H. Bouchiat, and R. Deblock, Phys. Rev. Lett. **108**, 046802 (2012).
[9] A. Eichler, M. Weiss, and C. Schönenberger, Nanotechnology **22**, 265204 (2011).
[10] A. Makarovski, A. Zhukov, J. Liu, and G. Finkelstein, Phys. Rev. B **75**, 241407(R) (2007).
[11] P. Jarillo-Herrero, J. Kong, H. S. J. van der Zant, C. Dekker, L. P. Kouwenhoven, and S. De Franceschi, Nature (London) **434**, 484 (2005).
[12] B. Babić, T. Kontos, and C. Schönenberger, Phys. Rev. B **70**, 235419 (2004).
[13] K. Kikoin, M. N. Kiselev, and Y. Avishai, *Dynamical Symmetries for Nanostructures* (Springer, Wien, 2012).
[14] K. Kikoin and Y. Avishai, Phys. Rev. Lett. **86**, 2090 (2001); Phys. Rev. B **65**, 115329 (2002).
[15] T. Kuzmenko, K. Kikoin, and Y. Avishai, Phys. Rev. Lett. **89**, 156602 (2002); Phys. Rev. B **69**, 195109 (2004).
[16] T. Kuzmenko, K. Kikoin, and Y. Avishai, Phys. Rev. Lett. **96**, 046601 (2006).

[17] T. Kuzmenko, K. Kikoin, and Y. Avishai, Phys. Rev. B **73**, 235310 (2006).
[18] H. Ajiki and T. Ando, J. Phys. Soc. Jpn. **62**, 1255 (1993).
[19] H. Ajiki and T. Ando, J. Phys. Soc. Jpn. **65**, 505 (1996).
[20] L. A. Chernozatonskii, P. B. Sorokina, E. E. Belova, J. Bruning, and A. S. Fedorov, JETP Lett. **85**, 77 (2007).
[21] M. Mirzadeh and M. Farjam, J. Phys.: Condens. Matter **24**, 235304 (2012).
[22] D. Goldhaber-Gordon, H. Shtrikman, D. Mahalu, D. Abusch-Magder, U. Meirav, and M. A. Kastner, Nature (London) **391**, 156 (1998); S. M. Cronenwett, T. H. Oosterkamp, and L. P. Kouwenhoven, Science **281**, 540 (1998).
[23] R. Egger, A. Zazunov, and A. L. Yeyati, Phys. Rev. Lett. **105**, 136403 (2010).
[24] R. Egger, A. Bachtold, M. S. Fuhrer, M. Bockrath, D. H. Cobden, and P. L. McEuen, in *Interacting Electrons in Nanostructures*, edited by R. Haug and H. Schoeller (Springer, Berlin, 2001), p. 125.
[25] O. Leenaerts, Ph.D. thesis, University of Antwerp, 2010.
[26] K. S. Kim, K. A. Park, H. J. Kim, D. J. Bae, S. C. Lim, Y. H. Lee, J. R. Kim, J.-J. Kim, and W. B. Choi, J. Korean Phys. Soc. **42**, S137 (2003).
[27] R. Balog, B. Jørgensen, L. Nilsson, M. Andersen, E. Rienks, M. Bianchi, M. Fanetti, E. Lægsgaard, A. Baraldi, S. Lizzit, Z. Sljivancanin, F. Besenbacher, B. Hammer, T. G. Pedersen, P. Hofmann, and L. Hornekær, Nat. Mater. **9**, 315 (2010).
[28] J. R. Schrieffer and P. A. Wolff, Phys. Rev. **149**, 491 (1966).
[29] A. C. Hewson, *The Kondo Problem to Heavy Fermions* (Cambridge University Press, Cambridge, 1993).
[30] B. Coqblin and J. R. Schrieffer, Phys. Rev. **185**, 847 (1969).
[31] A. Kaminski, Yu. V. Nazarov, and L. I. Glazman, Phys. Rev. B **62**, 8154 (2000).
[32] V. T. Rajan, Phys. Rev. Lett. **51**, 308 (1983).
[33] H. C. Manoharan, C. P. Lutz, and D. M. Eigler, Nature (London) **403**, 512 (2000); V. W. Brar, R. Decker, H.-M. Solowan, Y. Wang, L. Maserati, K. T. Chan, H. Lee, C. O. Girit, A. Zettl, S. G. Louie, M. L. Cohen, and M. F. Crommie, arXiv:1006.1014.
[34] A. Jerez, N. Andrei, and G. Zaránd, Phys. Rev. B **58**, 3814 (1998).
[35] B. Uchoa, T. G. Rappoport, and A. H. Castro Neto, Phys. Rev. Lett. **106**, 016801 (2011).
[36] Proof of the statement that $K_{1\alpha\alpha'}$ and $K_{2\alpha\alpha'}$ do not depend on λ is similar to the proof that P_1 and P_2 do not depend on λ, Appendix C 2.